Hysteretic Feedback Control of Electrostatic Levitator for Objects Possessing Large Suspension Area-Airgap Ratio

Shao Jü Woo[1)], Jong Up Jeon[2)], Toshiro Higuchi[3)], and Andreas Stemmer[1)]

[1)] Institute of Robotics, Nanotechnology Group
Swiss Federal Institute of Technology Zurich (ETHZ)

[2)] Samsung Advanced Institute of Technology, Samsung Corp., South-Korea

[3)] Department of Precision Machinery Engineering, University of Tokyo, Japan

ABSTRACT

This paper proposes a structurally simple stabilizing hysteretic feedback controller for contactless electric suspension devices in an effort to render electrostatic levitation technology more industrially attractive. The main system features of the proposed hysteretic feedback control-based levitator are: (i) its simple relay-based hardware realization, (ii) complete obsoleteness of dc high-voltage amplifiers, and (iii) its cost-effective and compact construction. Instead of dc high-voltage amplifiers only a maximum number of two high-voltage power sources capable of delivering a dc voltage are required. Despite the occurrence of limit cycles inherent to any relay switching control scheme, a stable and excellent performance in terms of position control can be obtained for the particular case of objects possessing a large suspension area-airgap ratio. The dynamics of the levitator is examined analytically and a closed-loop stability analysis is conducted using the describing function method. The effectiveness of the proposed controller was experimentally investigated on a prototype electrostatic levitation device for contactless suspension of a 4-inch silicon wafer.

I. INTRODUCTION

Electrostatic levitation offers the advantage to directly suspend a wide variety of materials without any direct mechanical contact, such as conductors, semiconductors, and dielectrics. This is in stark contrast with the well known and established electromagnetic levitation technology [1] which is limited to contactless suspension of ferromagnetic media only while electrostatic levitation technology allows the suspension of dielectric and semiconducting media as well. Despite these advantages, the application of electrostatic levitation technology has not had the success of its electromagnetic counterpart. Two major reasons for this can be attributed to the fact that electrostatic levitation exhibits low suspension force output levels and necessitates the formation of strong electric fields between the stator electrodes and the suspended object [2]. The latter is achieved by supplying high-voltages, typically in the kV range, to the stator electrodes in combination with small airgaps. An upper limit, however, exists for the magnitude of the stator electrode voltage and is dictated by the Passchen electric field break-down strength in ambient air. This restriction along with the fact that the total electrostatic suspension force is proportional with the suspension area of the object, leads to the conclusion that thin objects, such as disk-shaped media and thin metal sheets, featuring large suspension area-airgap ratios are most relevant to be suspended. Since most electric suspension systems are open-loop unstable, dynamic stabilization is necessary which is usually achieved by means of a feedback controller which regulates the suspension force by using the position of the suspended object measured at discrete locations as feedback signal. The feedback controller may regulate all six degrees of freedom (DOF) of the suspended object, however, more often only a reduced number of DOF's are controlled while the remaining ones are passively stabilized. Kumar *et al*. [3] succeeded in contactless suspension of a rotor in micro-electric bearings where the rotor consisted of a microscope cover slide covered with a thin copper layer. Electric field traps [4] and miniaturized-electrode arrays [5] have been used to handle, position, and transport dielectric particles and biological cells suspended in dielectric media by using dielectrophoretic forces. Kaler *et al*. [6] used feedback-controlled dielectrophoretic forces generated by a cone-plate electrode structure to stably levitate single biological cells. More recently, electric suspension of a 4-inch silicon wafer [7, 8] and quartz glass panels [9] have been reported as well. Upon reviewing the electrostatic suspension systems reported in the open literature it was found that the majority of them deploy dc high-voltage amplifiers as a means of amplifying the low output voltage signals of the feedback controller to the suspension voltages. Indeed, the overall cost and dimensions of electrostatic suspension devices are dominated by the dc high-voltage amplifiers which are costly and comparatively bulky components. Since the required number of dc high-voltage amplifiers is proportional to the number of electrodes to be controlled, extreme system costs can be expected to arise in applications deploying distributed electrode systems for

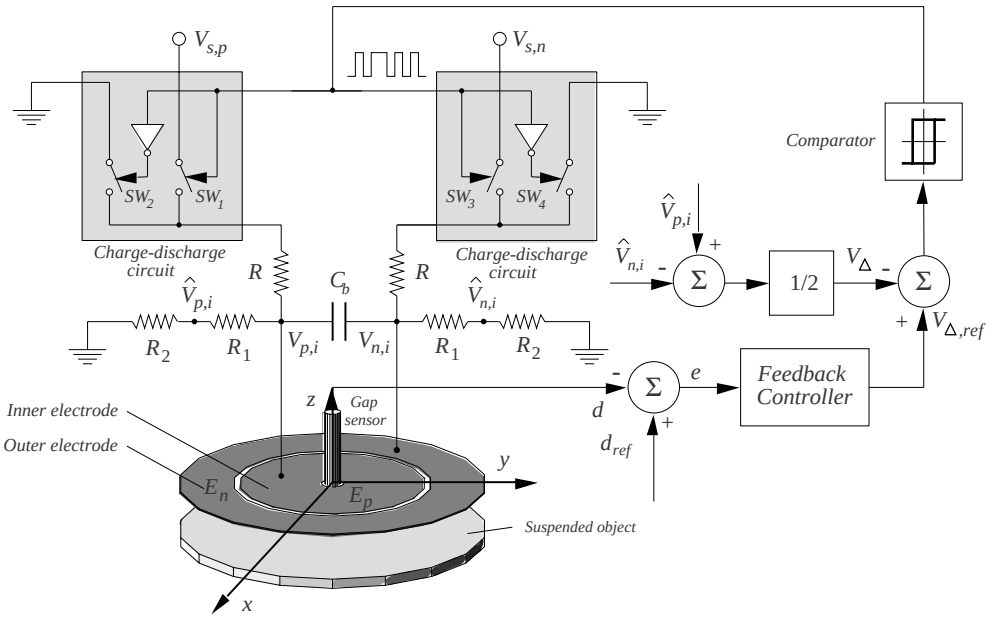

FIGURE 1: One-degree of freedom electrostatic levitator

the suspension of, e.g., flexible bodies. These drawbacks have seriously hampered widespread industrial application. To address the identified cost and complexity problem, a hysteretic feedback controller is proposed for the suspension of disk-shaped objects. In the domain of electromagnetic bearings hysteresis amplifiers have been used to control the switching times of switching power amplifiers which deliver the necessary ampere-order bearing coil currents. The main feature of the hysteretic feedback controller is that neither high-voltage amplifiers nor power amplifiers are required. Instead, independent from the number of electrodes to be controlled, only up to two dc high-voltage supplies are needed. In addition, its simple and low-cost relay-based hardware realization contributes highly to a cost-effective, compact, and non-complex electrostatic suspension system.

II. Principle of Operation

A. One-degree of Freedom Electrostatic Levitator

Fig. 1 depicts the model of an one-degree of freedom (DOF) electrostatic levitator which will be used to elucidate the operational principle of the proposed controller. For simplicity, a disk-shaped object is taken as the object to be suspended. The stator electrode structure consists of two concentric electrodes whose overall diameter is the same as that of the suspended disk. The inner and outer electrodes form variable parallel-type of plate capacitors with the suspended object. Furthermore, a gapsensor is placed at the geometrical center of the stator for the purpose of continuously measuring the position d of the suspended disk. Based on the deviation of d from the reference position d_{ref}, a feedback controller outputs a stabilizing reference electrode voltage signal $V_{\Delta,ref}$. The comparator incorporating hysteresis acts to switch on/off the dc supply voltages $V_{s,p}$ and $V_{s,n}$ to the electrodes to ensure that the electrode voltage V_Δ tracks $V_{\Delta,ref}$ globally. Electric charging of the electrodes is performed by closing switches SW_1 and SW_4 while discharging is performed by closing switches SW_2 and SW_3. The basic configuration consisting of the inner and outer electrode, and the charge-discharge circuit will referred to as an electrode unit. Rather than applying the supply voltages directly to the electrodes, they are applied as terminal voltages to a *RC*-type of circuit consisting of external resistors R, R_1 and R_2, and capacitor C_b in order to prevent the occurrence of high switching frequencies which may shorten the life span of the switches. The resulting switching frequency is a function of R, R_1, R_2, C_b, C_p, C_n, and the hysteresis of the comparator. Since the magnitudes of the electrode voltages V_p and V_n are too high to be used in the low voltage electronic control circuitry, a simple pull-down network consisting of R_1 and R_2 is utilized. The pulled-down electrode voltages are then converted to V_Δ. In the particular case when the two conditions: (i) equal suspension areas of the inner and outer electrodes and (ii) application of an anti-symmetrical supply voltage distribution, i.e., $V_{s,p}$ =-$V_{s,n}$, are fulfilled, a disk potential of zero will be obtained. The first condition implies that the capacitance C_p between the positively charged electrode and the suspended disk is approximately equal to the capacitance C_n between the negatively charged electrode and the suspended disk. This result can be easily verified from the following expression for the electric potential ϕ_d of the disk:

$$\phi_d = \frac{C_p V_p + C_n V_n}{C_p + C_n} \approx \frac{C_p V_p + C_p(-V_p)}{C_p + C_p} = 0 \qquad (1)$$

This particular condition is highly desired in clean-room applications where contamination of the suspended object has to be strictly avoided. A nonzero potential of the suspended object would result in attraction of contaminating foreign particulates through electrostatic effects. Clean-room applications which could benefit from this condition are, e.g., in the area of silicon wafer and Liquid Crystal Display (LCD) processing. Concerning the positioning control performance, relay based control inevitably introduces persistent oscillations in the disk's position. The amplitudes of these limit cycles depend on the supply voltage magnitudes, hysteresis, *RC* values, and the squeeze airfilm damping. Since the latter depends strongly on the airgap separation and the disk velocity, a relatively strong passive damping force can be obtained. This damping force has the same order of magnitude as the electrostatic suspension force and, thus, contributes in a convenient way to limit cycle suppression.

B. Three-degrees of Freedom Electrostatic Levitator

The transition of an one-DOF levitator to one which can suspend an object in five degrees of freedom, i.e., the longitudinal and lateral position in the plane of the object, the position of the object's center of mass (z), and its pitch (θ) and roll angle (ξ), can be done in a straightforward fashion. In actual applications only the three degrees of freedom z, θ, and ξ need to be actively controlled since the remaining ones are passively stabilized through electrostatic restriction forces arising from edge effects [2]. Fig. 2 shows an electrode pattern structure which could be used for a three-DOF levitator configuration. The electrode pattern consists of three electrode units each of which determine their control actions on the basis of the local airgap lengths measured by the associated gap sensors. Clearly, this configuration leads to a decentralized control structure which greatly contributes to simplifying the hardware realization of the levitator.

III. Electromechanical Model

As a typical electromechanical system an electrostatic suspension system can be described by an algebraic force transmission relationship, and the mechanical and electrical subsystem dynamics.

A. Algebraic Force Transmission Relationship

The electrostatic forces produced by each stator electrode can be derived from a variable capacitance model. The variable capacitances are formed between the inner and outer electrodes of each electrode unit where the suspended object acts to couple the electric field between these electrodes. By assuming a uniform electric field between the suspended object and the stator electrodes, the electrostatic forces can be derived easily. This assumption is justified when the ratio of the airgap length and the

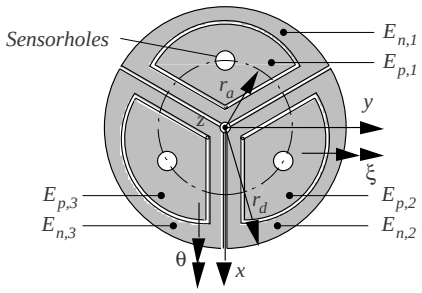

FIGURE 2: Electrode pattern for three-DOF electrostatic levitator

overlapping area between object and stator is very small. As a consequence, the capacitances C_i, i=1,2,3, between the inner and outer electrode at electrode unit i, can be written as $C_i = (1/4)\varepsilon A_i d_i^{-1}$ where ε represents the permittivity of the surrounding medium, A_i is the total area of the electrode unit, and d_i is the airgap length. Now, the attractive electric force $F_{e,i}$ can be calculated by integrating the surface electric force density $f_{e,i}$ over the suspension area of unit electrode i:

$$\boldsymbol{F}_{e,i} = \int_{A_i} \boldsymbol{f}_{e,i}\, dA = \int_{A_i} \sigma_i \boldsymbol{E}_i dA = \frac{\varepsilon A_i V_i^2}{8 d_i^2} \boldsymbol{e}_z \qquad (2)$$

where σ_i is the surface charge density, V_i=$V_{p,i}$-$V_{n,i}$, and E_i represents the uniform electric field strength.

B. Mechanical Subsystem Dynamics Analysis

The nonlinear rigid body equations of motion of the suspended disk can be conveniently derived using the Lagrange formalism. The generalized coordinates in this derivation are the actively controlled degrees of freedom of the disk: z, θ, and ξ. As a result, the following three coupled nonlinear second-order differential equations are obtained:

$$\begin{aligned} m\ddot{z} + mg &= Q_z - F_d \\ \ddot{\theta}(I_x \cos^2\xi + I_z \sin^2\xi) + \dot{\theta}\dot{\xi}\sin 2\xi (I_z - I_x) &= Q_\theta \\ 2I_x\ddot{\xi} - \frac{\dot{\theta}^2}{2}\sin 2\xi (I_z - I_x) &= Q_\xi \end{aligned} \qquad (3)$$

where m represents the mass of the disk, I_x and I_y are the moments of inertia about the z- and x-axis, respectively, g is the gravitational constant, F_d represents the damping force, and Q_z, Q_θ and Q_ξ are the generalized forces associated with the generalized coordinates q_z=z, q_θ=θ, and q_ξ=ξ, respectively. These generalized forces can be calculated from:

$$Q_k = \sum_{j=1}^{3} \boldsymbol{F}_{e,j} \cdot \frac{\partial \boldsymbol{r}_j}{\partial q_k}, \qquad k = z, \theta, \xi \qquad (4)$$

where $\boldsymbol{r}_j$ is the position vector associated with the geometrical center of the jth electrode unit, and $\boldsymbol{F}_{e,j}$ is the electric force exerted on the disk by the jth electrode unit. Evaluation of Eq. (3) yields:

$$Q_z = \sum_{j=1}^{3} \boldsymbol{F}_{e,j}$$

$$Q_\theta = \frac{1}{2} r_a \{ (\sin\theta\sin\xi + \sqrt{3}\cos\theta)(\boldsymbol{F}_{e,3} - \boldsymbol{F}_{e,2}) - 2\boldsymbol{F}_{e,1} \sin\theta\sin\xi \} \quad (5)$$

$$Q_\xi = \frac{1}{2} r_a \cos\xi\cos\theta(2\boldsymbol{F}_{e,1} - \boldsymbol{F}_{e,2} - \boldsymbol{F}_{e,3})$$

where r_a is the radius of the circle circumscribing the geometrical centers of the electrode units. The external damping force F_d originating from the squeeze film damping can be formally found by solving the Navier-Stokes equation. However, obtaining a closed-form analytical solution for this equation for the case that the disk has non-zero angular rotations θ and ξ is very difficult. Hence, it is assumed that these rotations are sufficiently small such that their influence on the squeeze film damping force can be neglected. The squeeze film damping is thus assumed to be caused predominantly by the disk's parallel motion with respect to the electrode surface. The resulting time-varying airgap leads to a symmetric air pressure distribution which is given by:

$$p(r, t) = \frac{3\eta_a(r^2 - r_d^2)}{z^3} \cdot \frac{\partial z}{\partial t} \quad (6)$$

where η_a represents the viscosity of ambient air, $\partial z/\partial t$ is the buffer velocity, r is the polar coordinate with respect to an inertial frame whose origin is located at the geometrical center of the stator, and r_d is the radius of the disk. Now, the nonlinear squeeze film damping force can be easily derived by integrating Eq. (5) over the suspension area of the disk:

$$F_d(z, t) = \int_0^{r_d} p(r, t) 2\pi r dr = \frac{3\pi\eta_a r_d^4}{2z^3} \cdot \frac{\partial z}{\partial t} \quad (7)$$

C. Electrical Subsystem Dynamics Analysis

Derivation of the equations describing the electrical subsystem dynamics amounts to finding the relationship between the voltage difference V_i=$V_{p,i}$-$V_{n,i}$, i=1,2,3, the applied voltages $V_{s,p}$ and $V_{s,n}$, and the disk's velocity and position. It is assumed that (i) the resistance of the cables and the switches through which the charge/discharge current flows to each electrode can be included in the resistance R, and (ii) the charging/discharging cycle of each electrode $E_{p,i}$ occurs simultaneously with that of it counterpart $E_{n,i}$. Now, from Fig. 1 one can find the following two general equations:

$$\frac{V_{s,p} - V_{p,i}}{R} = \frac{\partial C_{t,i}(V_{p,i} - V_{n,i})}{\partial t} + \frac{V_{p,i}}{R_m} \quad (8)$$

$$\frac{V_{n,i} - V_{s,n}}{R} = \frac{\partial C_{t,i}(V_{p,i} - V_{n,i})}{\partial t} - \frac{V_{n,i}}{R_m} \quad (9)$$

where $C_{t,i}$=C_b+$C_{p,i}C_{n,i}(C_{p,i}$+$C_{n,i})^{-1}$ and R_m=R_1+R_2, i=1,2,3. Using Eqs. (8) and (9) one can readily show that the electrical charging dynamics are governed by the following nonlinear differential equation:

$$V_{s,p} - V_{s,n} = R\left\{ V_i \left(2\frac{\partial C_{t,i}}{\partial t} + \frac{1}{R_m} + \frac{1}{R} \right) + 2C_{t,i}\frac{\partial V_i}{\partial t} \right\} \quad (10)$$

In the special case that $C_{p,i}$=$C_{n,i}$ and $V_{s,p}$=-$V_{s,n}$=V_{on} during the charging cycle, Eq. (10) becomes:

$$V_{on} = R\left\{ \frac{V_i}{2}\left(\frac{1}{R_m} + \frac{1}{R} - \frac{\varepsilon A_i}{2d_i^2}\frac{\partial d_i}{\partial t} \right) + \left(C_b + \frac{\varepsilon A_i}{4d_i} \right)\frac{\partial V_i}{\partial t} \right\} \quad (11)$$

The resistor network consisting of R_1 and R_2 pulls the high-voltages $V_{p,i}$ and $V_{n,i}$ existing at the inner and outer electrodes down to $\hat{V}_{p,i}$ and $\hat{V}_{n,i}$:

$$\hat{V}_{p,i} = \frac{R_2}{R_m} V_{p,i} \ , \quad \hat{V}_{n,i} = \frac{R_2}{R_m} V_{n,i} \quad (12)$$

D. Linearized Open-loop Dynamics

Eqs. (2), (3), (5), (7), and (10) provide a full description of the open-loop electromechanical dynamics of the proposed electric suspension device. In general, one may find that in practical devices the airgap and electrode voltage fluctuations around their reference values are very small. This fact suggests that the electromechanical model may be simplified by subjecting it to a linearization procedure around the reference point characterized by position $d_{i,0}$ and electrode voltage $V_{\Delta,0}$. In this section, the general case of $C_{p,i}$≠$C_{n,i}$ and $|V_{s,p}| \neq |V_{s,n}|$, is abandoned in favor of the practically more interesting set of system parameters $C_{p,i}$=$C_{n,i}$,$V_{s,p}$=-$V_{s,n}$=V_{on}, and A_i=A. Let Δd_i, Δz, $\Delta\theta$, $\Delta\xi$, and $\Delta V_{\Delta,i}$ denote small perturbations from the reference values $d_{i,0}$=d_0, z_0, θ_0, ξ_0, and $V_{\Delta,0}$, respectively. Furthermore, let $V_{\Delta,ref,i}$ denote the output voltage of the feedback controller and $\Delta V_{\Delta,R,i}$ denote the ripple present in $\Delta V_{\Delta,i}$, i=1,2,3, caused by the switching actions. Now, straightforward calculation yields the linearized open-loop electromechanical model given by:

$$M\ddot{\boldsymbol{r}} = \boldsymbol{w} + 3K_s C_s \boldsymbol{r} - C_d\dot{\boldsymbol{r}} + K_v C_v \upsilon \quad (13)$$

$$\dot{\upsilon} - R\tau_v^{-1}K_v T_c \dot{\boldsymbol{r}} = \tau_v^{-1}\{ \boldsymbol{u}_e - \alpha_1(\boldsymbol{v}_{\Delta,0} + \upsilon) \} \quad (14)$$

where we define the following vector and parameter identities:

$$\boldsymbol{r} = \begin{bmatrix} \Delta z & \Delta\theta & \Delta\xi \end{bmatrix}^{\mathrm{T}}, \ \upsilon = \begin{bmatrix} \Delta V_{\Delta,1} & \Delta V_{\Delta,2} & \Delta V_{\Delta,3} \end{bmatrix}^{\mathrm{T}},$$

$$\boldsymbol{v}_{\Delta,ref} = V_{\Delta,0}\begin{bmatrix} 1 & 1 & 1 \end{bmatrix}^{\mathrm{T}}, \ \boldsymbol{d} = \begin{bmatrix} \Delta d_1 & \Delta d_2 & \Delta d_3 \end{bmatrix}^{\mathrm{T}},$$

$$\boldsymbol{w} = \begin{bmatrix} \frac{\varepsilon A}{2d_0^2}\sum_{i=1}^{3} V_{\Delta,0}^2 - mg & 0 & 0 \end{bmatrix}^{\mathrm{T}}, \ \alpha_2 = \frac{3\pi\eta_a r_d^4}{2d_0^3},$$

$$\boldsymbol{u}_e = \left[u_{1,k}\ u_{2,k}\ u_{3,k}\right]^{\mathrm{T}},\ \alpha_1 = \frac{R}{R_m} + 1,\ \tau_v = 2R\left(\frac{\varepsilon A}{4d_0} + C_b\right),$$

$$k_v = \frac{\varepsilon A}{d_o^2} V_{\Delta,0}\ ,\ k_s = -\frac{\varepsilon A}{d_o^3} V_{\Delta,0}^2$$

and the following matrix definitions which include the mechanical damping matrix C_d, mass matrix M, and the linearized transformation matrix T_c which transforms $\boldsymbol{r}$ to $\boldsymbol{d}$ according to $\boldsymbol{d} = T_c \boldsymbol{r}$:

$$M = \begin{bmatrix} m & 0 & 0 \\ 0 & I_x & 0 \\ 0 & 0 & I_x \end{bmatrix},\ C_d = \alpha_2 \begin{bmatrix} 1 & 0 & 0 \\ 0 & 0 & 0 \\ 0 & 0 & 0 \end{bmatrix},\ C_s = \frac{1}{2} \begin{bmatrix} 2 & 0 & 0 \\ 0 & r_a^2 & 0 \\ 0 & 0 & r_a^2 \end{bmatrix},$$

$$T_c = \frac{r_a}{2} \begin{bmatrix} 2r_a^{-1} & 0 & 2 \\ 2r_a^{-1} & -3^{1/2} & -1 \\ 2r_a^{-1} & 3^{1/2} & -1 \end{bmatrix},\ C_v = \frac{r_a}{2} \begin{bmatrix} 2r_a^{-1} & 2r_a^{-1} & 2r_a^{-1} \\ 0 & -3^{1/2} & 3^{1/2} \\ 2 & -1 & -1 \end{bmatrix}$$

It should be noted that the vector $\boldsymbol{u}$ contains the externally applied voltage $u_{i,k}$, i=1,2,3, k=0,1, which equals V_{on} when charging is commanded (k=1) and zero when discharging is commanded (k=0). Here the voltage $V_{\Delta,0}$ is chosen such that, when applied to an electrode unit, one third of the weight of the suspended object is balanced at the reference position, which implies $\boldsymbol{w}$=0.

E. Closed-loop Dynamics and Stability Analysis

The open-loop system is closed and stabilized by introducing a suitable feedback controller into the loop. In many cases, a conventional Proportional-Integral-Derivative (PID) controller is sufficient to obtain good positioning performance. In this paper, a PD controller is adopted as stabilizing feedback controller. Addition of integral control would reduce or eliminate steady-state errors. Now, the resulting closed-loop system dynamics can be obtained by substituting the decentralized feedback law

$$\boldsymbol{v}_{\Delta,ref} = -(K_p \boldsymbol{e} + K_d \dot{\boldsymbol{e}}) \tag{15}$$

into Eqs. (13) and (14) where the error $\boldsymbol{e}$ is given by:

$$\boldsymbol{e} = \left[\Delta d_{ref} - \Delta d_1\ \Delta d_{ref} - \Delta d_2\ \Delta d_{ref} - \Delta d_3\right]^{\mathrm{T}} \tag{16}$$

The following stability analysis is carried out for the one-DOF levitator shown in Fig. 1. For this levitator, the feedback law given in Eq. (15) simplifies to the scalar law $V_{\Delta,ref} = -(K_p(\Delta d_{ref} - \Delta d) + K_d(\Delta \dot{d}_{ref} - \Delta \dot{d})$. An approximate stability and limit cycle analysis of the one-DOF suspension device can be conducted by determining the describing function N of the nonlinear relay [8], which amounts to finding the complex ratio of the fundamental harmonic component of its output to its input signal. Fig. 3 shows a block diagram of the one-DOF closed-loop system where it is assumed that the relay incorporates a hysteresis band h and a time delay $e^{-\tau s}$, which reflects the switch-on/off delays of the actual switches used in the prototype electric suspension device. The Fourier transform of the linearized open-loop electromechanical model of the one-DOF levitator is given by:

$$\Delta d(j\omega) = \frac{3k_v \Delta V_\Delta(j\omega)}{m(j\omega)^2 + \alpha_2 j\omega - 3k_s} \tag{17}$$

$$\Delta V_\Delta(j\omega) = \frac{u_k - \alpha_1 V_{\Delta,0} + \frac{R}{2} k_v j\omega \Delta d(j\omega)}{\alpha_1 + j\omega\tau_v} \tag{18}$$

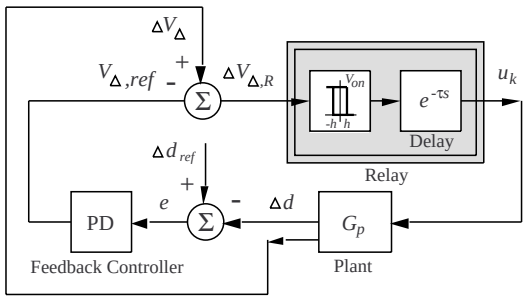

FIGURE 3: Block diagram of closed-loop system

The describing function $N(j\omega)$ of the relay incorporating an additional time delay $e^{-\tau s}$ can be derived as:

$$N(j\omega) = \frac{-2V_{on}}{\pi \left\| \Delta V_{\Delta,R}(j\omega) \right\|} e^{-j\left\{\sin^{-1}\left(\frac{h}{\left\| \Delta V_{\Delta,R}(j\omega) \right\|}\right) + \tau\omega\right\}} \tag{19}$$

Now, by substituting the relation

$$u_k = N(j\omega)(\ \Delta V_\Delta(j\omega) - V_{\Delta,ref}(j\omega)\ ) \tag{20}$$

into the Fourier transform of Eqs. (17) and (18) and solving the resulting set of equations for $\Delta d(j\omega)$ and $\Delta V_\Delta(j\omega)$, the closed-loop transfer function can be derived as:

$$\Delta d(j\omega) = \frac{3K_v(\ \alpha_1 V_{\Delta,o} - \Delta d_{ref}(K_p + j\omega K_d)\ )}{b_3(j\omega)^3 + b_2(j\omega)^2 + b_1 j\omega + b_0} \tag{21}$$

where

$$b_3 = \tau_v m,\ b_2 = \alpha_2 \tau_v + m(N - \alpha_1),$$

$$b_1 = -\left(3K_s\tau_v - \alpha_2(N - \alpha_1) + 3K_v\left(K_d - \frac{R}{2}K_v\right)\right),$$

$$b_o = -(3K_s(N - \alpha_1) + 3K_v K_p$$

The limit cycle amplitudes and the frequencies at which they occur can be found by solving the following two equalities for $\left\| \Delta V_{\Delta,R}(j\omega) \right\|$ and ω:

$$\mathrm{Re}(\ b_3(j\omega)^3 + b_2(j\omega)^2 + b_1 j\omega + b_0) = 0 \tag{22}$$

$$\mathrm{Im}(\ b_3(j\omega)^3 + b_2(j\omega)^2 + b_1 j\omega + b_0) = 0 \tag{23}$$

Based on this solution, it can be easily shown that for the on/off delays of the actual switches and an appropriate choice of PD control parameters and hysteresis h, the closed-loop system and, thus, the limit cycles are stable.

IV. Experimental Results

A three-DOF prototype electrostatic levitator has been constructed for the suspension of a 4-inch silicon wafer and incorporates the stator electrode pattern design shown in Fig. 2 and the proposed hysteretic feedback controller. The stator electrode has an outer diameter matching that of the silicon wafer and was fabricated using a standard wet etching technique. Sensor openings lying on a circle with a radius of 28 mm are provided in the electrode for mounting the PHOTONICS optical fiber gapsensors. The highly compact hysteretic feedback controller circuitry uses inexpensive AQV258 photomos relays, which can handle input voltages up to 1.5 kV. Both stator electrode and gapsensors are mounted on an aluminum base plate which is supported by three micrometer screws. The silicon wafer is supported below the stator electrode by three micrometer screws as well. Table 1 shows the system and control parameters.

TABLE 1:
Control and system parameters

K_p	$0.5 \cdot 10^7$ V/m	R	20 MΩ
K_i	$1 \cdot 10^8$ V/ms	R_1	40 MΩ
K_d	$1.5 \cdot 10^6$ Vs/m	R_2	1 MΩ
$V_{\Delta,o}$	357.6 V	C_b	235 pF
V_{on}	860 V	τ	0.4 ms
d_o	200 µm	h	2 V

Fig. 4 shows the recorded transient airgap variations Δd_i with respect to the reference airgap and the electrode voltages $V_{\Delta,i}$, i=1,2,3, when the silicon wafer was lifted from its support. As can be observed, the response characteristics of all three airgap variations are well damped and show no overshoots. Due to the noise present in the sensor signals and the switch-on/off time delays of the photomos switches, the ripple in the steady-state airgap lengths have amplitudes of approximately 2 µm, which can be reduced by selecting better switches.

V. Conclusions

A stabilizing hysteretic feedback controller for contactless electric suspension has been presented in this paper. Its simple and cost-effective relay-based hardware realization, and the complete obsoleteness of dc high-voltage amplifiers lead to a great reduction in system complexity and costs relative to existing electrostatic suspension systems. Instead of dc high-voltage amplifiers only a maximum number of two dc high-voltage power source are required. The dynamics of the levitator have been examined analytically using the describing function method and shows that the closed-loop system is stable. The successful contactless suspension of a 4-inch silicon wafer in ambient air on a prototype suspension device shows the effectiveness of the proposed controller.

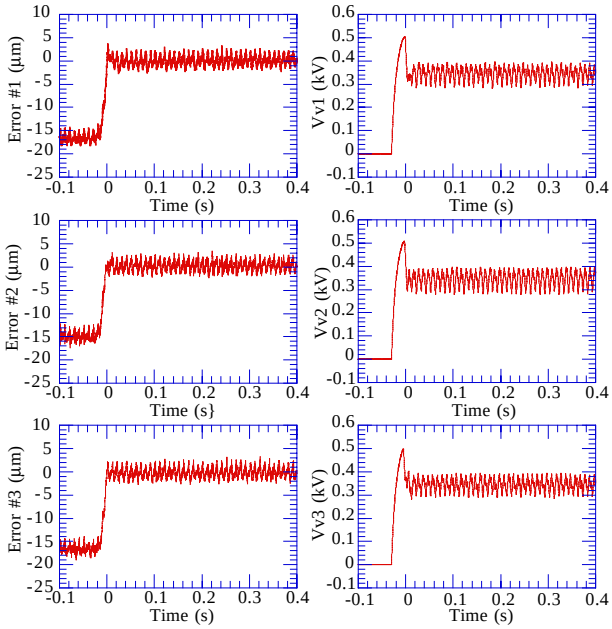

FIGURE 3: Measured airgap variations Δd_i with respect to the reference airgap length and electrode voltages $V_{v,i}$, i=1,2,3

The experimental results also demonstrate that despite the limit cycle behavior inherent to the use of relays, a stable and good performance in terms of position control can be obtained for the particular case of objects possessing a large suspension area-airgap ratio.

VI. References

[1] G. Schweitzer, H., Bleuler, and A. Traxler, *Active Magnetic Bearings*, Berlin: Springer-Verlag, 1993.

[2] S.J. Woo, J.U. Jeon, T. Higuchi, and J. Jin, "Electrostatic force analysis of electrostatic levitation system," *Proc. 34th SICE Annual Conf.*, Hokkaido, Japan, pp. 1347-1352, July 1995.

[3] S. Kumar, D. Cho, and W.N. Carr,"Experimental study of electric suspension for microbearings," *J. of Microelectromechanical systems*, Vol. 1, No.1, pp. 23-32, March 1992.

[4] T. Schnelle, R. Hagedorn, G. Fuhr, and T. Müller, "Three-dimensional electric field traps for manipulation of cells-calculation and experimental evaluation," *Biochimica et Biophysica Acta*, vol. 1157, No. 1, pp. 127-140, 1993.

[5] M.P. Hughes, R. Pethig, X.B. Wang, "Dielectrophoretic forces on particles in traveling electric fields," *J. Phys. D:Appl. Phys.*, Vol. 29, pp. 474-482, 1996.

[6] K.V.I.S. Kaler, J-P. Xie, T.B. Jones, and R. Paul, "Dual-frequency dielectrophoretic levitation of Canola protoplasts," *Biophys. J.*, Vol. 63, pp. 58-69, 1992.

[7] J. Jin, T. Higuchi, and M. Kanemoto, "Electrostatic silicon wafer suspension," *Proc. 4th Int. Symp. Magnetic Bearings*, ETH Zürich, Switzerland, pp. 343-348, August 1994.

[8] S.J. Woo, J.U. Jeon, and T. Higuchi, "A simple and cost-effective electrostatic levitator for disk-shaped objects," *Proc. IEEE/ASME Int. Conf. Advanced and Intelligent Mechatronics*, Tokyo, Japan, June 1997.

[9] J.U. Jeon, S.J. Woo, and T. Higuchi, "Electrostatic suspension of glass plate," *Proc. 11th KACC*, Pohang, South-Korea, pp. 267-270, October 1996.